https://doi.org/10.5194/egusphere-2024-2264
Preprint. Discussion started: 16 September 2024

Characterization of fog microphysics and their relationships with visibility at a mountain site in China

Quan Liu[1], Xiaojing Shen[1,*], Junying Sun[1,*], Yangmei Zhang[1], Bing Qi[2], Qianli Ma[3], Lujie Han[3], Honghui Xu[3], Xinyao Hu[1], Jiayuan Lu[1], Shuo Liu[1], Aoyuan Yu[1], Linlin Liang[1], Qian Gao[4], Hong Wang[1], Huizheng Che[1], Xiaoye Zhang[1]

[1] State Key Laboratory of Severe Weather & Key Laboratory of Atmospheric Chemistry of CMA, Chinese Academy of Meteorological Sciences, Beijing, 100081, China

[2] Hangzhou Meteorological Bureau, Hangzhou, 310051, China

[3] Lin'an Atmosphere Background National Observation and Research Station, Lin'an, 311307, Hangzhou, China

[4] Beijing Weather Modification Center, Beijing, 100089, China

Correspondence to: Xiaojing (shenxj@cma.gov.cn) and Junying Sun (jysun@cma.gov.cn)

Abstract. Enhancing the understanding of fog microphysical processes is essential for reducing uncertainty in fog forecasts, particularly in predicting fog visibility and duration. To investigate the complex interactions between aerosols and fog microphysics and their impacts on visibility degradation, simultaneous measurements of aerosol and fog microphysical characteristics were conducted from April to May, 2023 at a mountain site (1483 m) in the Yangtze River Delta (YRD) region, China. During this campaign, 8 fog events were explored, revealing significantly higher fog droplet number concentrations (N_d) compared to those observed in clean areas. A strong correlation was found between pre-fog aerosol number concentration (N_a) and the peak N_d of each fog event, indicating the substantial influence of pre-existing aerosol levels on fog microphysics. Water vapor supersaturation ratio (*SS*) within fogs was estimated to 0.07%±0.02%, slightly higher than previous estimates in urban and suburban areas. The broadening of the droplets size distribution (DSD) at stages of formation, development, and mature were dominantly driven by activation, condensation, collision-coalescence mechanism, respectively. This evolution process often led to a shift from unimodal to trimodal DSD, with peaks observed around 6, 12, and 23 μm. For fog events occurring under high N_a background, a notable decrease of temperature during mature stage promoted a secondary activation-dominated process, resulting in the formation of numerous small fog droplets and reducing large droplet size. The evolution of DSD can significantly influence visibility (*VIS*) in fogs. Detailed comparison of several visibility calculation methods suggests that estimating visibility based on the extinction of fog droplets only led to considerable overprediction when 100 m < $VIS \leq$ 1000 m. The results highlight the necessity of incorporating both fog droplet and aerosol extinction in fog visibility forecasts, particularly in anthropogenically polluted regions.

https://doi.org/10.5194/egusphere-2024-2264
Preprint. Discussion started: 16 September 2024

1 Introduction

Fog, consisting of suspended liquid droplets or ice crystals near the ground, has substantial impacts on transportation, aviation, and daily activities due to its capability to drastically reduce visibility to less than 1 km (Koračin et al., 2014; Niu et al., 2010a; Gultepe et al., 2015). The formation and types of fog are influenced by various atmospheric conditions and processes. For instance, continental fog commonly forms by radiative cooling of the surface (known as radiation fog) or through the lowering of pre-existing stratus clouds to ground level (Tardif and Rasmussen, 2007). Maritime fog generally forms when warm and moist air flows over a cooler water surface (Pilié et al., 1979). Once the fog forms, its life cycle is influenced by a combination of radiation, turbulence, thermodynamic, and cloud microphysical processes (Mazoyer et al., 2017). These processes interact in complex manners that are not yet fully understood. Advancing the understanding of fog microphysical processes is essential for improving fog forecasts (Martinet et al., 2020; Boutle et al., 2015), particularly in predicting the timing of fog formation and dissipation (Van Der Velde et al., 2010; Boutle et al., 2018).

Aerosol particles can serve as cloud condensation nuclei (CCN) in supersaturated water vapor environments (Twomey, 1959), playing an important role in the evolution of fog. The concentration, size distribution, and chemical composition of aerosols can significantly influence fog microphysical characteristics and optical properties (Twomey, 1977; Dusek et al., 2006; Zhao and Garrett, 2015). For example, in regions with intense anthropogenic activities, the abundance of CCN can lead to the formation of numerous but smaller fog droplets (Li et al., 2017; Twomey, 1977) and prolonging fog atmospheric lifetime (Yan et al., 2020; Jia et al., 2019). This can enhance the light scattering, thereby reducing visibility more effectively than that in cleaner environments with fewer but larger droplets. Additionally, the activation capacity of aerosol particles is mainly determined by their size distribution and chemical composition (Andreae and Rosenfeld, 2008; Gysel et al., 2007). Particles with high activation capacity can lower the critical activation supersaturation threshold needed for droplet formation (Zhang et al., 2012; Ervens et al., 2005). Therefore, the influence of aerosols on fog microphysics varies across regions with different aerosol backgrounds.

Given that visibility degradation is the most significant hazard during fog events, accurately estimating visibility is crucial for fog prediction. Numerous previous studies have focused on the relationship between fog microphysical parameters and visibility. Eldridge (1961) identified a strong negative correlation between fog visibility (*VIS*) and liquid water content (*LWC*) based on fog observations (Eldridge, 1961). In addition to *LWC*, Meyer et al. (1980) suggested that there is a significant negative correlation between fog *VIS* and droplet number concentration (N_d) (Meyer et al., 1980). Kunkel (1984) suggested that *LWC* could serve as the single parameter for visibility parameterization for fog, based on observation data of 11 fog cases. To improve fog visibility predictions, a dual-parameters scheme ($LWC \cdot N_d$), relating both of *LWC* and N_d to *VIS*, was proposed and optimized by Gultepe et al. (2006). This dual-parameters scheme demonstrated higher forecast accuracy compared to the *LWC*-only scheme (Zhang et al., 2014). Additionally, Song et al. (2019) suggested that *VIS* is not only related to $LWC \cdot N_d$ but also to the effective diameter (D_{eff}) of droplet size spectrum (Song et al., 2019). They incorporated D_{eff} into the dual-parameter scheme based on fog observations in the mountainous regions of Korea. Zhang et al. (2014)

https://doi.org/10.5194/egusphere-2024-2264
Preprint. Discussion started: 16 September 2024

examined these parameterization methods using in situ measurement data from four fog cases in a region of intense anthropogenic emissions, and they found that these parameterizations were unsuitable for light fog events.

To improve the understanding of the interactions between aerosols and fog microphysics and their impacts on visibility degradation in polluted regions, simultaneous measurements of number size distributions of aerosol particle and fog droplet were conducted at a mountain site in the megacity cluster of the YRD region, China. In this study, eight fog events are discussed in detail to illustrate the potential impacts of different aerosol concentration background on fog microphysical characteristics. The applicability of several fog visibility parameterization schemes for this region was compared and optimized. Furthermore, to highlight the significant impact of aerosol extinction under light fog conditions in polluted region, the contributions of aerosols and droplets to visibility during different stages of fog evolution were also discussed.

2 Measurement and methodology

2.1 Observation site

Simultaneous measurements of aerosol particle number size distribution (PNSD), CCN number concentration, and fog microphysical parameters (N_d, LWC, D_{eff}) were conducted during April 11th to May 8th, 2023 at the summit of Mt. Daming in Hangzhou, China. The mountain site (30.03°N, 119.00°E, 1483 m a.s.l.) locates in the southwest Hangzhou area with a distance of ~120 km from Hangzhou downtown (Fig. S1), belonging to the YRD region. The surroundings of this site have no distinct anthropogenic emissions apart from a few villages at the base of the mountain. Due to the unique geography, the site frequently experiences various cloud/fog events (Fig. 1a), such as orographic cloud, radiation fog, and stratus-lowering fog. Additionally, Sun et al. (2018) had reported the mean values of the PBL height in Hangzhou were approximately 1.5 km during the warmer months (including April to May). The heigh of this site is generally near the top of the planetary boundary layer (PBL) around midday, and thus can be influenced by surface anthropogenic emissions through daytime convective mixing or regional transport from surrounding megacities.

2.2 Instrumentation and Methods

2.2.1 Sampling inlet system

To simultaneously measure the physicochemical properties of fog interstitial particles and fog residual particles, an automatic three-way switching inlet system was developed, incorporating a $PM_{2.5}$ cyclone and a Ground-based Counterflow Virtual Impactor (GCVI) (model 1205, Brechtel Manufacturing Inc., USA). This system utilized two electromagnetic ball valves installed in the $PM_{2.5}$ cyclone and GCVI air pathways, respectively, and was controlled by a custom LabView (National Instruments, Austin, USA) software. The inlet system was installed on the roof, approximately 3 m above the ground. The aerosol measurements were performed downstream of this inlet system, including PNSD, CCN concentration at different water vapor saturation (SS), and aerosol chemical composition. The switching method is controlled automatically

https://doi.org/10.5194/egusphere-2024-2264
Preprint. Discussion started: 16 September 2024

based on fog and fog-free conditions. Fog condition was detected by using visibility and RH sensors integrated into the GCVI system, with thresholds set at 1000 m for visibility and 95% for RH. Under fog-free conditions, ambient air was sampled through the $PM_{2.5}$ inlet and dried by an automatic regenerating absorption aerosol dryer, ensuring the relative humidity (RH) in the sample flow remained below 30% (Tuch et al., 2009). Under fog conditions, the sampling system alternated between the $PM_{2.5}$ cyclone and GCVI pathways every 30 minutes. During fog events, particles collected through the $PM_{2.5}$ cyclone pathway represent unactivated fog interstitial particles, while particles sampled and dried via the GCVI pathway represent fog droplet residual particles.

The GCVI system uses a compact wind tunnel placed upstream of the CVI inlet (model 1204) to accelerate cloud/fog droplets into the CVI inlet tip. Droplets smaller than the cut size of CVI inlet are rejected from the tip by the counterflow. Droplets larger than the cut size but smaller than the maximum size limit pass through the tip and are dried into small residue particles. For a given counterflow, airspeed within the wind tunnel, temperature, and pressure, the cut size of droplet that penetrates into the inlet is fixed. In this study, the GCVI inlet sampled droplets with aerodynamic diameters larger than 7.8 μm by setting the airspeed and counter flow to 90 m s^{-1} and 4 L min^{-1}, respectively. The droplets were then dried using an evaporation chamber (airflow temperature at 40 ℃) in the GCVI. Details of the GCVI system can be found in other studies (Shingler et al., 2012; Bi et al., 2016). It is worth noting that the GCVI tends to yield a higher number concentration of cloud particles compared to the actual ambient cloud particle concentration, which should be corrected using an enrichment factor (EF). The EF was calculated based on the GCVI sampling flow settings, airspeed, and its geometry configuration, as recommended by Shingler et al. (2012). In this work, an EF of 6.01 was derived for airspeed of 90 m s^{-1}. Therefore, the concentration measured at the downstream of the GCVI pathway has been corrected by the EF of 6.01.

2.2.2 Fog microphysical parameters

A Fog Monitor (Model FM-100, DMT Inc., USA) was applied in situ for measuring real-time DSD within the size range of 2-50 μm. The inlet of FM-100 sampled air approximately 2.5 m above the ground. Droplets are sorted into the 20 predefined size bins with a measuring time-resolution of 1 s. The values of fog microphysical parameters (N_d, LWC, and D_{eff}) were calculated from fog DSD according to the equations addressed by Spiegel et al. (2012):

$$N_d = \sum N_i \quad (1)$$

$$LWC = \frac{\pi}{6} \sum N_i D_i^3 \rho_w \quad (2)$$

$$D_{eff} = \sum N_i D_i^3 / \sum N_i D_i^2 \quad (3)$$

where N_i is the droplet number concentration in the ith bin, D_i denotes the diameter in the ith bin, and ρ_w = 1 g cm^{-3} represents for the density of pure water.

2.2.3 Aerosol measurements

The dry PNSDs were measured by a Twin Scanning Mobility Particle Sizer (TSMPS, TROPOS, Germany), consisting of a

https://doi.org/10.5194/egusphere-2024-2264
Preprint. Discussion started: 16 September 2024

Differential Mobility Analyzer (DMA) and a Condensation Particle Counter (CPC, Model 3772, TSI Inc., USA). The TSMPS system measured the PNSD within the range 10-850 nm in mobility diameter with an X-ray neutralizer. Each scan was set to 5 min for every loop with a total sample flowrate of 2.5 L min^{-1}.

The CCN number concentration (N_{CCN}) was measured at various *SS* using a Cloud Condensation Nuclei Counter (Model CCN-100, DMT Inc., USA). In this study, the CCN counter was sequentially set to four supersaturation (*SS*) values: 0.1%, 0.2%, 0.4%, and 0.7%, each for a duration of 5 minutes, with a complete cycle lasting 20 minutes. Due to the cloud chamber inside the CCN counter requires time to stabilize the temperature after each change in *SS*, data measured in the first minute of each *SS* were excluded. The ratio of sample flow and sheath flow was set at 1:10, with the flowrate of 0.45 L min^{-1} and 4.5 L min^{-1}, respectively. The *SS* calibration of CCNc-100 was performed with ammonium sulfate particles before and after the campaign.

Aerosol chemical components were measured by a high-resolution time-of-flight aerosol mass spectrometer (HR-ToF-AMS, Aerodyne Inc., USA) (Canagaratna et al., 2007; Decarlo et al., 2006), including nitrate, sulfate, chloride, ammonium, and organics. Black carbon (BC) mass concentrations were obtained by using a single particle soot photometer (SP2, DMT Inc., USA) (Schwarz et al., 2006; Liu et al., 2020a). The aerosol chemical compositions in this study were used to derive their hygroscopic parameter (κ) following the method by Liu et al. (2023). Detailed analysis on chemical properties of cloud interstitial particles and droplet residual particles will be presented in a subsequent study.

2.2.4 Definition of fog event

The definition of fog event in this study requires the following conditions to be met simultaneously: visibility less than 1000 m, relative humidity greater than 95%, and fog droplet number concentration greater than 10 cm^{-3}. Intervals between fog events need to include at least three consecutive hours of fog-free period. In order to avoid precipitation interference in fog measurements, those processes in which fog appeared after precipitation were eliminated from the later analysis. Hereby, there were 8 available fog events in total were selected to analyze in following text. The detail description for the eight fog events was summarized in Table 1.

3 Results and discussions

3.1 Overview of the observation

Fig. 1 shows the temparal variations of meteorological parameters, cloud microphysical parameters, and aerosol size distribution measured in the field observation from April 11th to May 8th, during which the 8 available fog events are observed. The temperature was above 0 ℃ during the entire observation period, indicating all of the observed fogs were warm fog processes. The wind speed and direction are shown by a polar plot of in Fig. S2. The prevailing wind direction throughout the study period was westerly, with strong winds (exceeding 8 m/s) primarily originating from the west and

https://doi.org/10.5194/egusphere-2024-2264
Preprint. Discussion started: 16 September 2024

southwest. In contrast, during foggy periods, the prevailing wind direction shifted to the northeast, with the main wind speeds ranging from 4 to 8 m/s.

Large ranges of fog microphysical parameters were observed during the campaign. The median values of N_d, *LWC* and D_{eff} of the 8 fog events varied over the ranges of 146–834 cm^{-3}, 0.009–0.216 g m^{-3}, and 5.5–12.2 μm, respectively (Table 1). The concentration levels of fog droplets varied by orders of magnitude in different environments, ranging from tens in marine and remote background environments (Duplessis et al., 2021; Gultepe et al., 2009) to hundreds in anthropogenically polluted environments (Li et al., 2020; Shen et al., 2018). The relationship between N_d and *LWC* for the 8 available fog events are presented in Fig. 2. There appears to be no direct correlation between the overall N_d and *LWC*. However, when binning N_d and *LWC* according to D_{eff} values, a notable high linear correlation showed up. This result indicates that using a single parameter to describe cloud microphysical properties may introduce significant uncertainty, which will be further discussed in detail in Section 3.5. For a given range of *LWC* values, N_d generally decreases as D_{eff} increases. This negative correlation between them is ubiquitous in fog, as the presence of more droplets competes for available water vapor, thereby inhibiting their growth (Li et al., 2017).

3.2 Relationship between pre-fog aerosols and fog droplets

Previous studies suggested the maximum N_d during cloud/fog formation period was not only depended on the *SS* reached by the air mass (Mazoyer et al., 2019; Pruppacher and Klett, 2010), but also had a high correlation between the pre-fog or cloud base aerosol number concentrations (N_a) (Duplessis et al., 2021; Hegg et al., 2012). Pre-fog N_a here was defined as the average of the last hour before fog formation. As it shown in Fig. 3a, the pre-fog N_{a_total} (integrated concentration from all size bins measured by TSMPS) had a high correlation with the peak N_d for these fog events, indicating the peak N_d was significantly influenced by pre-fog aerosol. Note that the pre-fog aerosols measured at the observation site may not fully represent the particles that actually activated into fog droplets. However, the observation results from the mountain site are regionally representative. Aerosol particles at this altitude level exhibit significant homogeneity in term of their physicochemical properties. For the fog events occurred after precipitation (hollow cycles in Fig. 3), the pre-fog N_a and did not follow this linear relationship. This further indicates that such processes should be removed from analysis of aerosol effects on fog microphysics.

The linear fitting slopes in Fig. 3, primarily depending on aerosol chemical composition and size distribution, can be used to associated with activation ratio of bulk aerosol. The slope value of 0.09 in this study is significantly higher than the 0.014 observed by Duplessis et al. (2021) on the eastern coast of Canada. In addition, the concentrations of particle diameter larger than 70 nm (N_{a_70}) or 100 nm (N_{a_100}) had a much stronger correlation with the peak N_d than that of total pre-fog N_a (Fig.S3 and Fig. 3b). Previous studies have reported that the peak SS expected in fogs are typically low (0.03–0.05%) (Mazoyer et al., 2019; Shen et al., 2018), indicating particles with a size smaller than 70 nm should not be activated in foggy conditions. The result suggests that a proper selection of particle size range is crucial for estimating the peak N_d by using pre-fog N_a.

https://doi.org/10.5194/egusphere-2024-2264
Preprint. Discussion started: 16 September 2024

3.3 Estimating water vapor supersaturation in fog

The *SS* in fogs, as one of the most important environmental parameters in response to fog evolution, cannot be directly measured. Aerosol particles will be activated when their critical activation *SS* lower than the maximum *SS* value of ambient air. In return, cloud/fog droplets can be formed by those particles whose diameters exceed the critical activation diameter (D_c) corresponding to that critical activation *SS*. In order to illustrate the influences of *SS* evolution on droplets size distribution, we used two approaches to derive SS. In the first approach, the averaged pre-fog PNSD represented the aerosol background before activation occurrence. The D_c here was determined as the particle size at which the N_d equaled to the integrated aerosol concentration of the pre-fog PNSD from the upper limit down to D_c (Fig. 4a). Then, the corresponding *SS* (SS_{PNSD}) was calculated by using the κ-Köhler equation (Petters and Kreidenweis, 2008) with an averaged κ of pre-fog aerosols. In the second approach, the N_d in the fog can be considered to be consistent with the activated CCN number concentration (N_{CCN}). The *SS* (SS_{CCN}) was derived from linear interpolation using the pre-fog *SS*-resolved N_{CCN} measurements (Fig. 4b). Due to the lowest *SS* setpoint in this study is 0.1%, *SS* values less than 0.1% were estimated from extrapolation of linear extension line (magenta dashed line in Fig. 4b), disregarding the non-linear relationship between them within the low *SS* range.

The time series of SS_{PNSD} and SS_{CCN} derived from above two approaches during a typical fog event are shown in Fig. 4c. Although their temporal variations exhibit a high consistence, the mean value of SS_{PNSD} is approximately 30% higher than SS_{CCN}. Because of much higher scanning resolution of particle size than that of SS in N_{CCN} measurements (four *SS* setpoints), and most SS_{CCN} values lower than the lowest *SS* setpoint (0.1%), substantial uncertainties were introduced by linear extrapolation when deriving SS_{CCN}. Therefore, the variations of SS_{PNSD} were considered to be closer to the actual situation and were used in subsequent discussions with a brief symbol of *SS*.

After fog formation, the *SS* had a strong negative correlation (r=-0.85, p<0.001) with ambient temperature (Fig. 4c and Fig. S4), indicating the decrease of temperature played a critical role in supplying sufficient *SS* for particles activation. Due to incomplete observation data of PNSD or DSD for several fog events during this campaign, here only five events with complete data of the entire process were selected for the SS statistics (Fig. 4d). The median *SS* values for each fog event varied in the range of 0.05%-0.13%, and the 95th quantile values were generally less than 0.1% except for the E4. During the whole observation period, the *SS* varied between 0.01% and 0.25%, with an average of (0.07±0.02)%, which is slightly higher than previously reported in urban (Shen et al., 2018), suburb (Mazoyer et al., 2019), and coast (Duplessis et al., 2021) environments, but significantly lower than that derived from aircraft measurements (Gong et al., 2023). The estimated *SS* in various observation environments seems to be positively correlated with altitude. It can partially be attribute to the lower aerosol number concentration and temperature at high altitudes (Liu et al., 2020b), which is apt to result in reduced water vapor consumption and the maintenance of a relatively high *SS* (Baccarini et al., 2020).

3.4 Temporal evolution of fog DSD

To explore the temporal evolution of fog, it is common to divide the process into various stages based on changes in

https://doi.org/10.5194/egusphere-2024-2264
Preprint. Discussion started: 16 September 2024

visibility. (Mazoyer et al., 2022; Niu et al., 2010b; Pilie et al., 1975). Upon this, each fog event in this study was divided into four stages, determined by the changes in visibility computed using a 15-minute sliding average (refer to the color-time divisions in Fig. 5). In the formation stage (blue line), there was a pronounced decline in visibility from 1000 to 100 meters within 20 minutes for all cases. In the development stage (magenta line), the visibility continued to decrease but at a significantly slower rate until reaching its minimum value. During the mature stage (brown line), the visibility undergone a slight increase or remains stable. Finally, during the dissipation stage (purple line), the visibility increased rapidly to 1000 meters.

As it shown in Fig. 5, two typical fog events, characterized by low and high pre-fog aerosol concentration conditions, were selected and analyzed in terms of the evolution of their microphysical characteristics. The averaged fog DSD during various stages are shown in Fig. 6. Analogous information for the other three fog events was presented in Fig. S5 and S6. Under low aerosol concentration background (E2), as the supersaturation ratio increases in the formation stage, N_d rapidly reached a peak within a short period, while both *LWC* and D_{eff} exhibited slow growth. This indicated that the fog droplets in this stage primarily formed through aerosol particle activation processes, which yielded small droplets with diameters less than 6 μm (Fig. 6a). During the development stage, the N_d continued to increase due to persistent activation of aerosol particles, along with both *LWC* and D_{eff} gradually increased to their maximum values. Another peak in the fog DSD emerges around 12 μm in this stage, indicating that the condensation process began to dominate the broadening of the DSD. In the subsequent mature stage, N_d experienced a significant decrease due to a substantial reduction in small droplets, then maintained a relatively stable value. Compared to the development stage, D_{eff} notably increased at this stage, with the main peak of the DSD shifted from 12 μm to 15 μm and an additional considerable peak appearing at 23 μm. These changes in fog microphysical characteristics suggest the occurrence of collision-coalescence process, leading to further broadening of the DSD towards larger sizes. After triggering the collision-coalescence mechanism, apart from small fog droplets, certain un-activated aerosol particles were scavenged by the uptake of larger fog droplets. This can be supported by variations of the activation ratio (AR) of cloud residual particles. The AR here was defined as the CCN number concentration at a *SS* setting of 0.2% relative to the total particle concentration. As shown in Fig. 7, the AR measured downstream of the GCVI airflow were closed to 1 when the D_{eff} smaller than 12 μm. However, when the collision-coalescence process occurred, indicated by D_{eff} exceeding 12 μm (Fig. 5c), the AR of cloud residual particles notably decreased. The reduced AR of cloud residual particles was caused by the uptake of particles less prone to activation into droplets, implying the removal efficiency for these particles significantly enhanced in this stage. Besides that, both *SS* and *LWC* fluctuate around a stable value in the mature stage, indicating that evaporation and condensation of water vapor were in a quasi-equilibrium state. In the dissipation stage, N_d and *LWC* decline rapidly to zero, with a gradual disappearance of droplets in the DSD from large to small sizes.

Under high aerosol concentration background (E3, in Fig. 5), the evolutions of fog microphysical characteristics during the formation and development stages were generally consistent with those in E2. However, after reaching and maintaining a quasi-equilibrium state (SS_{Q1}) in the early mature stage, a notable decrease of temperature caused a further increase in

https://doi.org/10.5194/egusphere-2024-2264
Preprint. Discussion started: 16 September 2024

supersaturation (Fig. 4c) and a new quasi-equilibrium (SS_{Q2}) with various fog microphysical characteristics. Compared to SS_{Q1}, the N_d substantially increased in the SS_{Q2} stage, while the *LWC* and D_{eff} notably decreased. The enhanced *SS* facilitated the further activation of smaller particles that were un-activated during the SS_{Q1} stage, resulting in a secondary activation-dominated process during the E3. Notably, the excess water vapor and water in liquid phase had been a quasi-equilibrium state during the SS_{Q1} stage. The new activated aerosol particles in the SS_{Q2} stage formed numerous small fog droplets and consumed the excess water vapor in fog, causing the partial pressure of water vapor in the gas phase to decrease. This leads to the evaporation of liquid water from previously formed large fog droplets, thereby reducing their size (Fig. 6b).

3.5 Links between fog microphysical parameters and visibility

3.5.1 Comparison of different fog visibility estimating methods

Given that visibility degradation is the primary hazard during fog events, establishing an appropriate visibility parameterization scheme in fog is crucial for improving the accuracy of fog visibility forecasts. The visibility of fog can be calculated from fog DSD (VIS_{DSD}), with

$$b_{ext} = \int Q_{ext} \frac{\pi}{4} D_i^2 N_i(D_i) dD_i \quad (4)$$

$$VIS_{DSD} = \frac{3.912}{b_{ext}} \quad (5)$$

Where b_{ext} is the extinction coefficient, Q_{ext} is the extinction cross section calculated by the droplet diameter (D_i) and wavelength of light (880 nm used in this study) using the Mie theory. This method incorporates a specific extinction algorithm based on physical processes. Thus, its calculation result is expected to be more consistent with actual condition, which can serve as a reference for the contribution of droplets to visibility. However, this method requires input of high-quality droplet spectrum data, thus limiting its application in fog prediction models. Previous studies have explored the relationship between fog microphysical parameters (i.e., *LWC*, N_d, and D_{eff}) and VIS_{DSD} (Gultepe et al., 2006; Song et al., 2019; Kunkel, 1984). A commonly used approach for estimating fog visibility was proposed by Kunkel (1984) as follow:

$$VIS_K = \frac{a}{LWC^b}, \; a = 0.021, \; b = 0.88 \quad (6)$$

This parameterization scheme is based only on *LWC* and is therefore widely applied in numerical models. However, the parameter of N_d can also significantly influence fog visibility. On this basis, the parameterization was developed by Gultepe et al. (2006) with utilizing both *LWC* and N_d:

$$VIS_G = \frac{c}{(LWC \cdot N_d)^d}, \; c = 1.002, \; d = 0.65 \quad (7)$$

The fitting parameters (*a*, *b*, *c*, *d*) in Equation (6) and (7) are influenced by the characteristics of fog DSD, and their values vary significantly in different regions and environments, with general ranges of 0.013-0.030 for *a*, 0.69-0.88 for *b*, 0.511-1.002 for *c*, and 0.51-0.65 for *d* (Kunkel, 1984; Gultepe and Milbrandt, 2007; Zhang et al., 2014). Such variability of these parameters emphasizes the strong regional dependence of the applicability of these two parameterization schemes. In this study, we re-established the parameters *a*, *b*, *c*, and *d* using our measured data. The reconstructed visibility calculations were

https://doi.org/10.5194/egusphere-2024-2264
Preprint. Discussion started: 16 September 2024

denoted as VIS_{KN} for the *LWC*-only parameterization and VIS_{GN} for the $LWC \cdot N_d$ parameterization. Fig. 8a presents a comparison of the calculated visibility based on different parameterization schemes with VIS_{DSD}. Compared to VIS_K and VIS_G, the deviations of VIS_{KN} and VIS_{GN} from VIS_{DSD} are significantly reduced, especially for VIS_{GN}, which has a linear fitting slope of 1.1. This indicates that the dual-parameters scheme of $LWC \cdot N_d$ can better describes visibility degradation contributed by fog droplets. As it shown in Fig. 3, when both *LWC* and N_d values are given, the information of D_{eff} can also be determined. Therefore, the $LWC \cdot N_d$ parameterization incorporates more information on fog microphysical characteristics and is expected to be more accurate.

To further evaluate the applicability of the *VIS* calculation methods mentioned above, we compared these calculated results with the visibility measured by a visibility sensor (Fig. 8b). The *LWC* and *VIS* exhibited an exponential relationship, with an inflection point appearing at ~100 m (Fig. S7). Accordingly, the relevant data were analyzed by dividing them into two intervals: $VIS_{obs} \leqslant 100$ m and 100 m < $VIS_{obs} \leqslant 1000$ m. The results showed that the visibility calculation methods used in Fig. 8b tended to be slightly overestimated to different degrees, with the linear fit slopes being 1.33 for VIS_{KN}, 1.16 for VIS_{GN}, and 1.21 for VIS_{DSD}. The dual-parameters method of $LWC \cdot N_d$ yielded a smaller deviation than that of the *LWC*-only method. However, when 100 m < $VIS_{obs} \leqslant 1000$ m, the *VIS* calculated from the three methods were substantially higher than VIS_{obs}, with no obvious correlations between them. This large difference was induced by the visibility data used for the development of visibility parameterizations relied on Mie calculations rather than observed results from a visibility sensor. Additionally, the parameterization schemes in those studies were derived from observations in relatively clean areas, where visibility degradation is predominantly caused by fog droplets. However, these schemes would induce in large uncertainties in visibility calculations in polluted areas, such as the North China Plain (Zhang et al., 2014), where aerosol concentration and extinction contribution can be much higher, especially in light fogs.

3.5.2 Aerosol effects on estimating fog visibility

To quantitatively estimate the aerosol contribution on visibility degradation in fog, the dry PNSD of cloud/fog interstitial particles was used to calculate their extinction. Due to the lack of aerosol particle hygroscopic growth factor of aerosol particles under supersaturated conditions, a rough estimation method was proposed to convert dry PNSD to ambient PNSD. This method was based on the continuity of the PNSD and assumed that the maximum dry particle size of fog interstitial particles, after hygroscopic growth under supersaturated conditions, corresponded to the cut-size of the sampling inlet ($PM_{2.5}$ cyclone). It also assumed that the hygroscopic growth factor was constant across different particle sizes. Based on these assumptions, the hygroscopic growth factor of particles under supersaturated conditions can be obtained (Fig. S8). Then the ambient aerosol contribution on visibility can be calculated based on Mie theory. The parameters relevant to the Mie calculations for aerosols are provided in Table S1.

Fig. 9 shows the comparison of visibility estimation based on only fog droplets and both fog droplets and interstitial particles, respectively. When $VIS_{obs} \leq 100$ m, the high concentration and large size of the fog droplets dominate the visibility

https://doi.org/10.5194/egusphere-2024-2264
Preprint. Discussion started: 16 September 2024

degradation. In this situation, the extinction effect of aerosols can be neglected. However, when 100 m < VIS_{obs} ≤ 1000 m, estimating visibility based on only fog droplet extinction led to substantial deviations, whereas considering both fog droplet and aerosol extinction significantly reduced the discrepancy between calculated and observed *VIS*. The comparison highlights the importance of considering both fog droplet and aerosol extinction in visibility forecasting during light fog conditions, particularly in polluted regions affected by anthropogenic emissions.

4 Conclusions and implications

To explore interactions between aerosols and fog microphysics and their impacts on visibility degradation, this study conducted simultaneous measurements of aerosol and fog microphysical characteristics in spring 2023 at the summit of Mt. Daming (1483 m), located in the YRD region, China. During this campaign, 8 fog events were observed. The median values of N_d, *LWC*, and D_{eff} for the 8 fog events varied within the ranges of 146–834 cm^{-3}, 0.009–0.216 g m^{-3}, and 5.5–12.2 μm, respectively. A strong correlation was found between pre-fog N_a and the peak N_d of each fog event, implying the potential influence of pre-existing aerosol levels on fog microphysics. Two approaches for deriving *SS* within fogs were proposed, based on measurements of PNSD and *SS*-resolved CCN concentration, respectively. The averaged *SS* for these fogs was estimated to 0.07%±0.02%, slightly higher than previous estimates in urban, suburban, and coast environments, but significantly lower than that derived from aircraft measurements. After fog formation, temperature reduction played a critical role in supplying sufficient *SS* for particles activation.

Each fog event was divided into formation, development, maturity, dissipation stages according to visibility variations. Various mechanism dominated the broadening of DSD at different stages, leading to a shift from a unimodal to a trimodal DSD, with peaks observed around 6, 12, and 23 μm. The formation of trimodal DSD was driven by collision-coalescence mechanism during the mature stage of fog, characterized by the D_{eff} exceeding 12 μm. Meanwhile, analysis on the activity of cloud residual particles suggests that apart from small fog droplets, certain un-activated aerosol particles were scavenged by the uptake of larger fog droplets in this stage. For fog events occurring under high N_a background, a notable decrease of temperature during mature stage promoted a secondary activation-dominated process, resulting in the formation of numerous small fog droplets and reducing large droplet size.

The visibility parameterization schemes based on fog microphysical parameters are widely used to estimate fog visibility. The fitting parameters of different *VIS* parameterization scheme were re-established based on our measuring data. The comparison results indicates that the dual-parameters scheme of $LWC \cdot N_d$ can better describes visibility degradation contributed by fog droplets. However, estimation of fog visibility based on only fog droplet extinction led to substantial deviations when 100 m < *VIS* ≤ 1000 m. The deviations were notably reduced by incorporating the extinction caused by fog interstitial particles. These findings emphasize the necessity of incorporating both fog droplet and aerosol extinction in fog visibility forecasts, particularly in regions impacted by anthropogenic pollution.

https://doi.org/10.5194/egusphere-2024-2264
Preprint. Discussion started: 16 September 2024

Data availability. All data in this paper are available from the authors upon request (liuq@cma.gov.com).

Author contributions. Conceptualization: QL and JS. Investigation: QL, XS, JS, YZ, BQ, QM, LH, HX, XH, JL, SL, and AY. Funding acquisition: QL, XS, and HC. Resource: QL, JS, XS, YZ, and XZ. Writing – original draft preparation: QL. All co-authors discussed the results and commented on the manuscript.

Competing interests. The authors declare that they have no conflict of interest.

Acknowledgments. This work was financially supported by the National Natural Science Foundation of China (grant nos. 42275121, 42030608) and the Chinese Academy of Meteorological Sciences (grant nos. 2023Z012, 2024Z006).

https://doi.org/10.5194/egusphere-2024-2264
Preprint. Discussion started: 16 September 2024

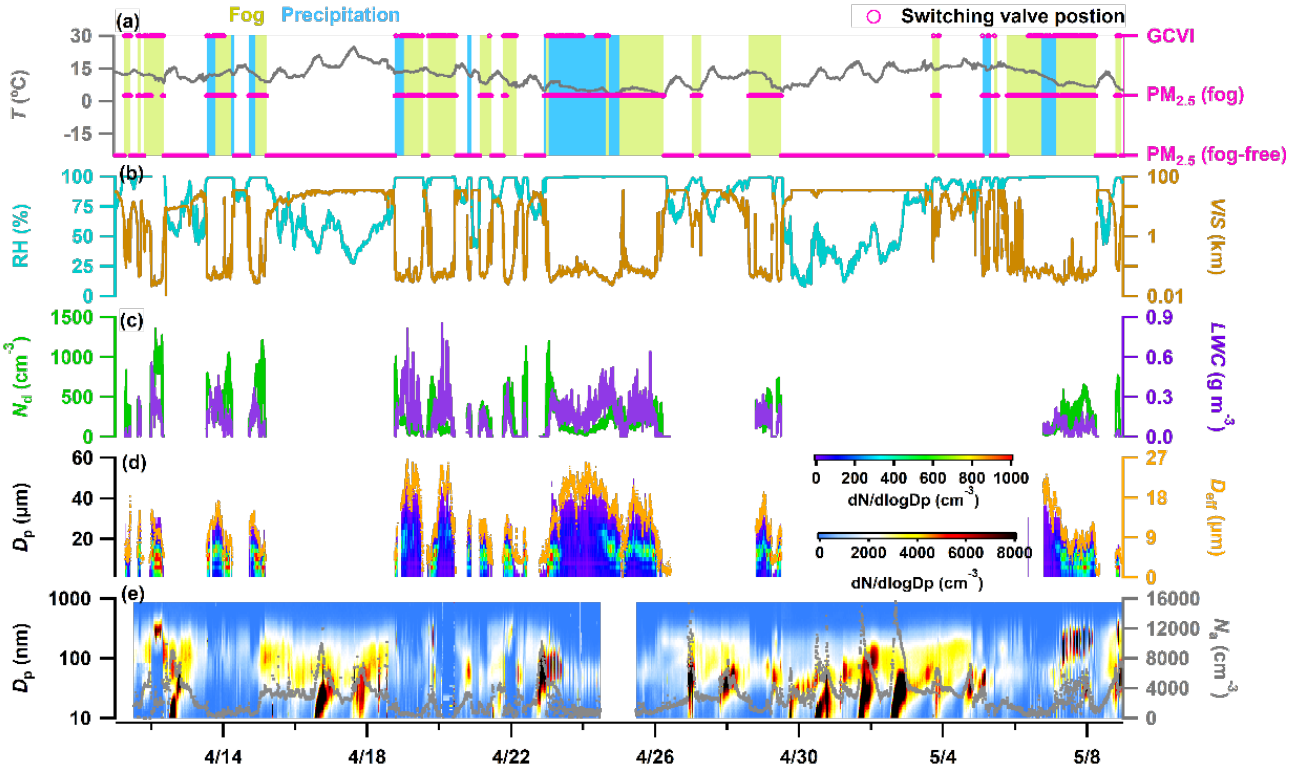

Fig. 1. Time series of (a) temperature (*T*), weather conditions and valve position of the switching inlet system, (b) relative humidity (RH) and visibility (*VIS*), (c) fog droplet number concentration (N_d) and liquid water content (*LWC*), (d) fog droplets size distribution and effective diameter (D_{eff}), and (e) number size distribution and number concentration (N_a) of dry aerosol particles, during this campaign.

https://doi.org/10.5194/egusphere-2024-2264
Preprint. Discussion started: 16 September 2024

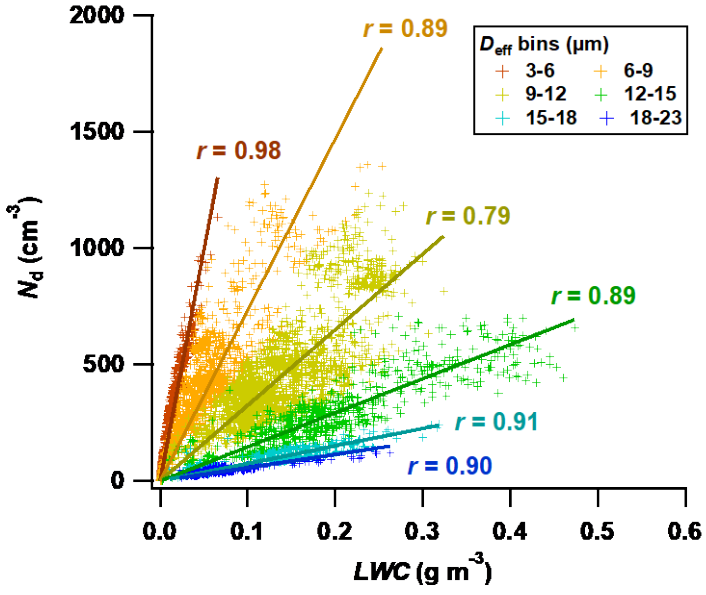

Fig. 2. Relationship between N_d and LWC within different D_{eff} bins.

370

https://doi.org/10.5194/egusphere-2024-2264
Preprint. Discussion started: 16 September 2024

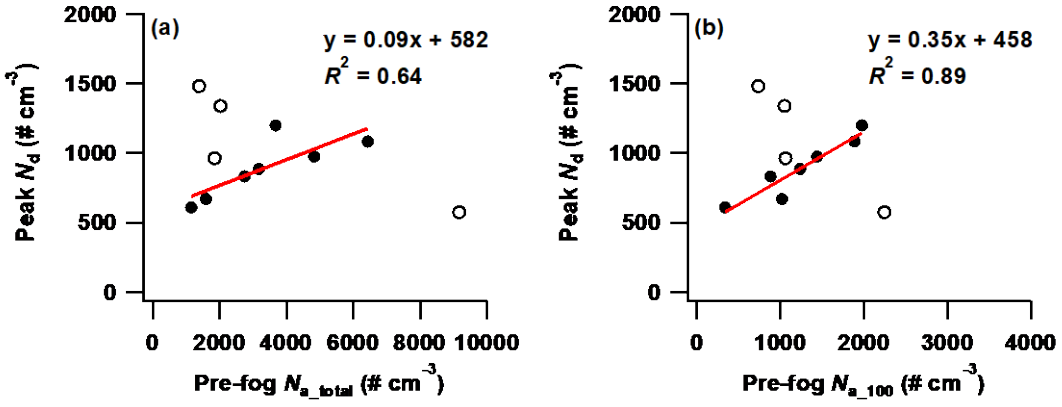

Fig. 3. Peak N_d value for each fog event versus averaged pre-fog N_a in the last hour before the event, measured by TSMPS within the ranges of (a) total measured sizes (10-850 nm) and (b) sizes larger than 100 nm. Hollow circles represent fog events occurring after precipitation, which are excluded from the correlation analysis.

375

https://doi.org/10.5194/egusphere-2024-2264
Preprint. Discussion started: 16 September 2024

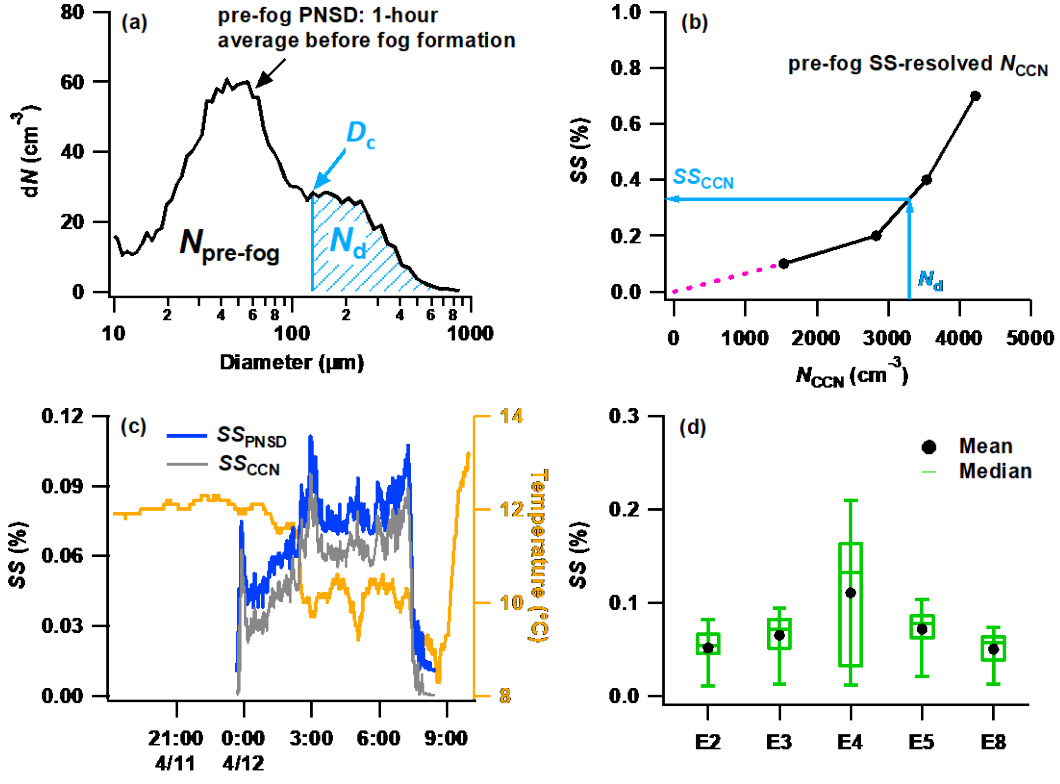

Fig. 4. Schematics of two methods for deriving water vapor supersaturation (*SS*) in fog, (a) SS_{PNSD} is derived from the averaged pre-fog particle number size distribution (PNSD) and N_d. The blue shaded area represents the integrated N_a from the upper end of the pre-fog PNSD to smaller sizes. The critical activation diameter (D_c) is defined as the diameter where the integrated N_a equals N_d. (b) SS_{CCN} is derived from the pre-fog SS-resolved N_{CCN} measurements and N_d. The magenta dashed line represents linear interpolation from N_{CCN} measurements at two lower SS setpoints. (c) Temporal variations of SS_{PNSD}, SS_{CCN}, and temperature during a typical fog event, (d) Statistics of *SS* for the five available fog events.

https://doi.org/10.5194/egusphere-2024-2264
Preprint. Discussion started: 16 September 2024

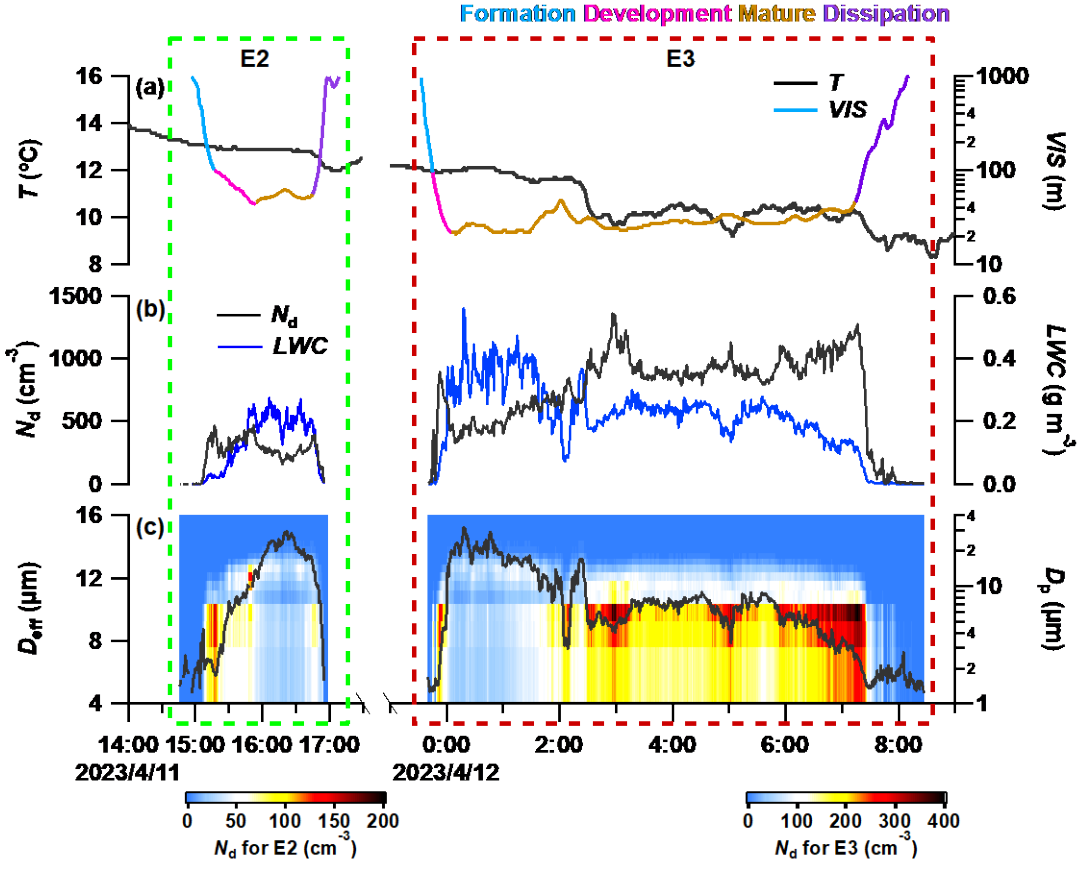

385 **Fig. 5. Temporal evolution of meteorological parameters and fog microphysical characteristics for two typical fog events, including (a) temperature (*T*) and visibility (*VIS*), (b) fog droplet number concentration (N_d) and liquid water content (*LWC*), (c) fog droplets size distribution and effective diameter (D_{eff}). E2 represents fog occurring under low pre-fog N_a background, while E3 represents fog occurring under high pre-fog N_a background. The colored lines separate each fog event into four stages based on the evolution of visibility.**

390

https://doi.org/10.5194/egusphere-2024-2264
Preprint. Discussion started: 16 September 2024

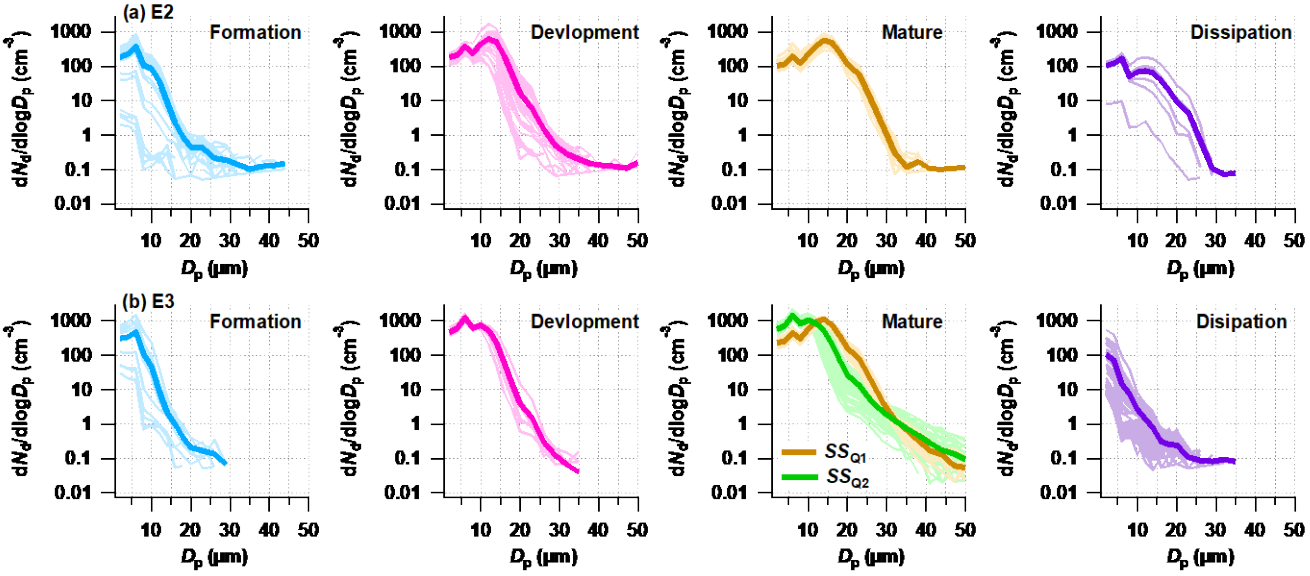

Fig. 6. Evolutions of fog droplets size distribution (DSD) at various stages during (a) E2 and (b) E3, respectively. Thin lines in each stage represent 1-min averaged DSDs, while the thick line is their average.

https://doi.org/10.5194/egusphere-2024-2264
Preprint. Discussion started: 16 September 2024

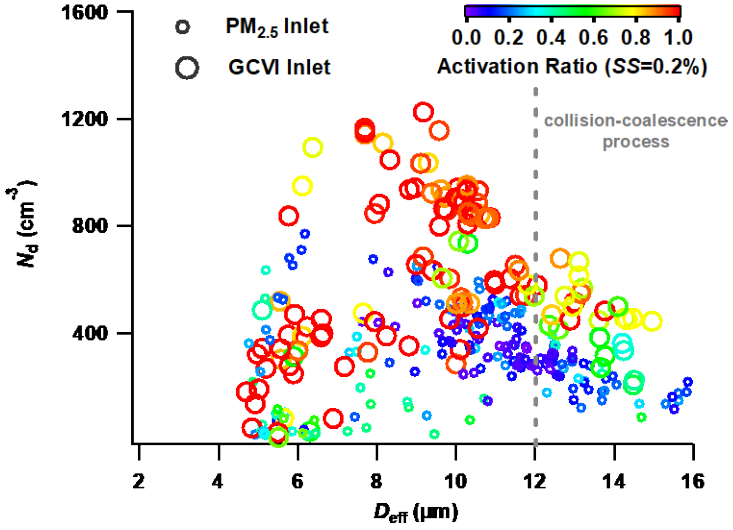

Fig. 7. Differences in CCN activity between fog residual particles (GCVI inlet) and fog interstitial particles ($PM_{2.5}$ inlet), and their variations with fog microphysical parameters. The gray dash line indicates significant collision-coalescence processes occurring when D_{eff} exceeds 12 μm.

https://doi.org/10.5194/egusphere-2024-2264
Preprint. Discussion started: 16 September 2024

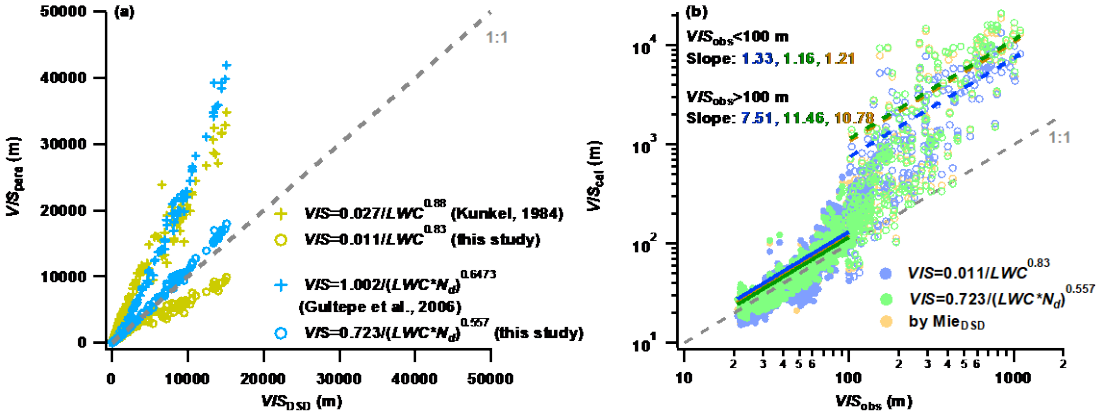

Fig. 8. Estimation of fog visibility using different calculation methods. (a) Comparison of various visibility parameterization schemes with that derived from droplets size distribution (VIS_{DSD}). (b) Relationship between calculated visibility (VIS_{cal}) and observed visibility (VIS_{obs}). Solid lines represent linear fits of different calculation methods with $VIS_{obs} \leq 100$ m, while dashed lines represent fits for 100 m $< VIS_{obs} \leq 1000$ m.

https://doi.org/10.5194/egusphere-2024-2264
Preprint. Discussion started: 16 September 2024

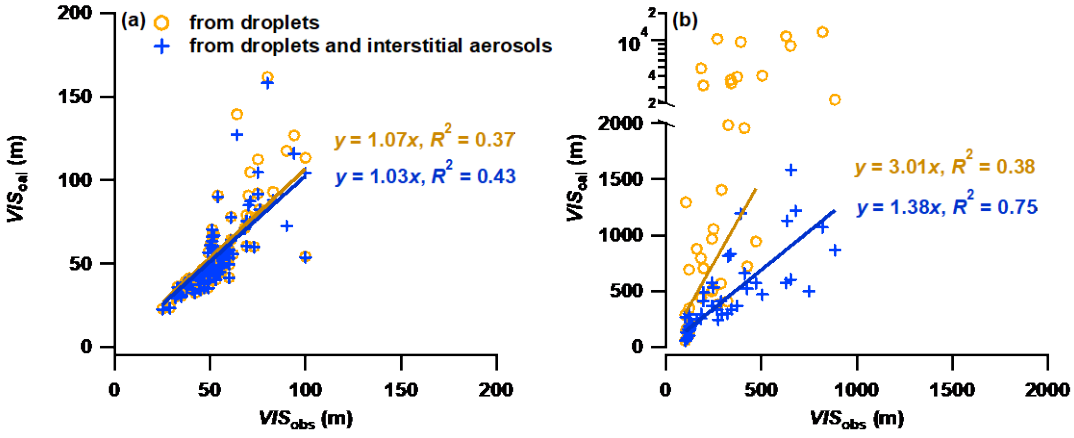

Fig. 9. Estimating visibility based on only fog droplets and both fog droplets and interstitial particles, respectively. (a) VIS_{obs}≤100 m; (b) 100 m < VIS_{obs}≤1000 m. Note that, values of VIS_{cal} larger than 2000 m have been excluded from the linear fit due to their substantial deviation.

410

https://doi.org/10.5194/egusphere-2024-2264
Preprint. Discussion started: 16 September 2024

Table 1 The median values of measured fog microphysical parameters for each fog event during the campaign.

Fog Events	N_d (# cm^{-3})	LWC (g m^{-3})	D_{eff} (μm)
E1 (04/11 06:08 – 10:16)	146	0.009	5.9
E2 (04/11 14:55 – 17:00)	276	0.167	12.2
E3 (04/11 23:40 – 04/12 08:25)	834	0.216	9.9
E4 (04/21 02:50 – 11:15)	305	0.107	10.6
E5 (04/21 18:46 – 04/22 03:50)	469	0.116	9.7
E6 (04/28 13:30 – 04/29 12:10)	312	0.160	11.6
E7 (05/06 18:50 – 05/08 05:55)	231	0.068	10.0
E8 (05/08 19:05 – 05/08 22:05)	504	0.025	5.5
Total	347	0.146	10.6

https://doi.org/10.5194/egusphere-2024-2264
Preprint. Discussion started: 16 September 2024

References

Andreae, M. and Rosenfeld, D.: Aerosol-cloud-precipitation interactions. Part 1. The nature and sources of cloud-active aerosols, Earth-Science Reviews, 13-41, 10.1016/j.earscirev.2008.03.001, 2008.

Baccarini, A., Karlsson, L., Dommen, J., Duplessis, P., Vüllers, J., Brooks, I. M., Saiz-Lopez, A., Salter, M., Tjernström, M., Baltensperger, U., Zieger, P., and Schmale, J.: Frequent new particle formation over the high Arctic pack ice by enhanced iodine emissions, Nature communications, 11, 4924, 10.1038/s41467-020-18551-0, 2020.

Bi, X., Lin, Q., Peng, L., Zhang, G., Wang, X., Brechtel, F. J., Chen, D., Li, M., Peng, P. a., Sheng, G., and Zhou, Z.: In situ detection of the chemistry of individual fog droplet residues in the Pearl River Delta region, China, Journal of Geophysical Research: Atmospheres, 121, 9105-9116, https://doi.org/10.1002/2016JD024886, 2016.

Boutle, I., Finnenkoetter, A., Lock, A., and Wells, O.: The London Model: Forecasting fog at 333 m resolution, Quarterly Journal of the Royal Meteorological Society, 142, 10.1002/qj.2656, 2015.

Boutle, I., Price, J., Kudzotsa, I., Kokkola, H., and Romakkaniemi, S.: Aerosol–fog interaction and the transition to well-mixed radiation fog, Atmos. Chem. Phys., 18, 7827-7840, 10.5194/acp-18-7827-2018, 2018.

Canagaratna, M. R., Jayne, J. T., Jimenez, J. L., Allan, J. D., Alfarra, M. R., Zhang, Q., Onasch, T. B., Drewnick, F., Coe, H., Middlebrook, A., Delia, A., Williams, L. R., Trimborn, A. M., Northway, M. J., DeCarlo, P. F., Kolb, C. E., Davidovits, P., and Worsnop, D. R.: Chemical and microphysical characterization of ambient aerosols with the aerodyne aerosol mass spectrometer, Mass Spectrometry Reviews, 26, 185-222, 10.1002/mas.20115, 2007.

DeCarlo, P. F., Kimmel, J. R., Trimborn, A., Northway, M. J., Jayne, J. T., Aiken, A. C., Gonin, M., Fuhrer, K., Horvath, T., Docherty, K. S., Worsnop, D. R., and Jimenez, J. L.: Field-Deployable, High-Resolution, Time-of-Flight Aerosol Mass Spectrometer, Analytical chemistry, 78, 8281-8289, 10.1021/ac061249n, 2006.

Duplessis, P., Bhatia, S., Hartery, S., Wheeler, M. J., and Chang, R. Y. W.: Microphysics of aerosol, fog and droplet residuals on the Canadian Atlantic coast, Atmospheric Research, 264, 105859, https://doi.org/10.1016/j.atmosres.2021.105859, 2021.

Dusek, U., Frank, G. P., Hildebrandt, L., Curtius, J., Schneider, J., Walter, S., Chand, D., Drewnick, F., Hings, S., Jung, D., Borrmann, S., and Andreae, M. O.: Size Matters More Than Chemistry for Cloud-Nucleating Ability of Aerosol Particles, Science, 312, 1375-1378, 10.1126/science.1125261, 2006.

Eldridge, R. G.: A few fog drop-size distributions, Journal of Atmospheric Sciences, 18, 671-676, https://doi.org/10.1175/1520-0469(1961)018<0671:AFFDSD>2.0.CO;2, 1961.

Ervens, B., Feingold, G., and Kreidenweis, S. M.: Influence of water-soluble organic carbon on cloud drop number concentration, Journal of Geophysical Research: Atmospheres, 110, https://doi.org/10.1029/2004JD005634, 2005.

Gong, X., Wang, Y., Xie, H., Zhang, J., Lu, Z., Wood, R., Stratmann, F., Wex, H., Liu, X., and Wang, J.: Maximum Supersaturation in the Marine Boundary Layer Clouds Over the North Atlantic, AGU Advances, 4, e2022AV000855, https://doi.org/10.1029/2022AV000855, 2023.

https://doi.org/10.5194/egusphere-2024-2264
Preprint. Discussion started: 16 September 2024

Gultepe, I. and Milbrandt, J. A.: Microphysical Observations and Mesoscale Model Simulation of a Warm Fog Case during FRAM Project, Pure and Applied Geophysics, 164, 1161-1178, 10.1007/s00024-007-0212-9, 2007.

Gultepe, I., Müller, M. D., and Boybeyi, Z.: A New Visibility Parameterization for Warm-Fog Applications in Numerical Weather Prediction Models, Journal of Applied Meteorology and Climatology, 45, 1469-1480, https://doi.org/10.1175/JAM2423.1, 2006.

Gultepe, I., Pearson, G., Milbrandt, J. A., Hansen, B., Platnick, S., Taylor, P., Gordon, M., Oakley, J. P., and Cober, S. G.: The Fog Remote Sensing and Modeling Field Project, Bulletin of the American Meteorological Society, 90, 341-360, https://doi.org/10.1175/2008BAMS2354.1, 2009.

Gultepe, I., Zhou, B., Milbrandt, J., Bott, A., Li, Y., Heymsfield, A. J., Ferrier, B., Ware, R., Pavolonis, M., Kuhn, T., Gurka, J., Liu, P., and Cermak, J.: A review on ice fog measurements and modeling, Atmospheric Research, 151, 2-19, 10.1016/j.atmosres.2014.04.014, 2015.

Gysel, M., Crosier, J., Topping, D. O., Whitehead, J. D., Bower, K. N., Cubison, M. J., Williams, P., Flynn, M., McFiggans, G., and Coe, H.: Closure Between Chemical Composition and Hygroscopic Growth of Aerosol Particles During TORCH2, Dordrecht, 731-735,

Hegg, D. A., Covert, D. S., Jonsson, H. H., and Woods, R. K.: A simple relationship between cloud drop number concentration and precursor aerosol concentration for the regions of Earth's large marine stratocumulus decks, Atmos. Chem. Phys., 12, 1229-1238, 10.5194/acp-12-1229-2012, 2012.

Jia, X., Quan, J., Zheng, Z., Liu, X., Liu, Q., He, H., and Liu, Y.: Impacts of Anthropogenic Aerosols on Fog in North China Plain, Journal of Geophysical Research: Atmospheres, 124, 252-265, https://doi.org/10.1029/2018JD029437, 2019.

Koračin, D., Dorman, C. E., Lewis, J. M., Hudson, J. G., Wilcox, E. M., and Torregrosa, A.: Marine fog: A review, Atmospheric Research, 143, 142-175, https://doi.org/10.1016/j.atmosres.2013.12.012, 2014.

Kunkel, B. A.: Parameterization of Droplet Terminal Velocity and Extinction Coefficient in Fog Models, Journal of Applied Meteorology, 23, 34-41, https://doi.org/10.1175/1520-0450(1984)023<0034:PODTVA>2.0.CO;2, 1984.

Li, J., Zhu, C., Chen, H., Zhao, D., Xue, L., Wang, X., Li, H., Liu, P., Liu, J., Zhang, C., Mu, Y., Zhang, W., Zhang, L., Herrmann, H., Li, K., Liu, M., and Chen, J.: The evolution of cloud and aerosol microphysics at the summit of Mt. Tai, China, Atmos. Chem. Phys., 20, 13735-13751, 10.5194/acp-20-13735-2020, 2020.

Li, S., Joseph, E., Min, Q., and Yin, B.: Multi-year ground-based observations of aerosol-cloud interactions in the Mid-Atlantic of the United States, Journal of Quantitative Spectroscopy and Radiative Transfer, 188, 192-199, https://doi.org/10.1016/j.jqsrt.2016.02.004, 2017.

Liu, D., Hu, K., Zhao, D., Ding, S., Wu, Y., Zhou, C., Yu, C., Tian, P., Liu, Q., Bi, K., Wu, Y., Hu, B., Ji, D., Kong, S., Ouyang, B., He, H., Huang, M., and Ding, D.: Efficient Vertical Transport of Black Carbon in the Planetary Boundary Layer, Geophysical Research Letters, 47, e2020GL088858, 10.1029/2020gl088858, 2020a.

https://doi.org/10.5194/egusphere-2024-2264
Preprint. Discussion started: 16 September 2024

Liu, Q., Shen, X., Li, L., Sun, J., Liu, Z., Zhu, W., Zhong, J., Zhang, Y., Hu, X., Liu, S., Che, H., and Zhang, X.: Impacts of Aerosol Chemical Composition on Cloud Condensation Nuclei (CCN) Activity during Wintertime in Beijing, China, Remote Sensing, 15, 10.3390/rs15174119, 2023.

Liu, Q., Liu, D., Gao, Q., Tian, P., Wang, F., Zhao, D., Bi, K., Wu, Y., Ding, S., Hu, K., Zhang, J., Ding, D., and Zhao, C.: Vertical characteristics of aerosol hygroscopicity and impacts on optical properties over the North China Plain during winter, Atmos. Chem. Phys., 20, 3931-3944, 10.5194/acp-20-3931-2020, 2020b.

Martinet, P., Cimini, D., Burnet, F., Ménétrier, B., Michel, Y., and Unger, V.: Improvement of numerical weather prediction model analysis during fog conditions through the assimilation of ground-based microwave radiometer observations: a 1D-Var study, Atmos. Meas. Tech., 13, 6593-6611, 10.5194/amt-13-6593-2020, 2020.

Mazoyer, M., Burnet, F., and Denjean, C.: Experimental study on the evolution of droplet size distribution during the fog life cycle, Atmos. Chem. Phys., 22, 11305-11321, 10.5194/acp-22-11305-2022, 2022.

Mazoyer, M., Lac, C., Thouron, O., Bergot, T., Masson, V., and Musson-Genon, L.: Large eddy simulation of radiation fog: impact of dynamics on the fog life cycle, Atmos. Chem. Phys., 17, 13017-13035, 10.5194/acp-17-13017-2017, 2017.

Mazoyer, M., Burnet, F., Denjean, C., Roberts, G. C., Haeffelin, M., Dupont, J. C., and Elias, T.: Experimental study of the aerosol impact on fog microphysics, Atmos. Chem. Phys., 19, 4323-4344, 10.5194/acp-19-4323-2019, 2019.

Meyer, M. B., Jiusto, J. E., and Lala, G. G.: Measurements of Visual Range and Radiation-Fog (Haze) Microphysics, Journal of Atmospheric Sciences, 37, 622-629, https://doi.org/10.1175/1520-0469(1980)037<0622:MOVRAR>2.0.CO;2, 1980.

Niu, S., Lu, C., Yu, H., Zhao, L., and Lü, J.: Fog research in China: An overview, Advances in Atmospheric Sciences, 27, 639-662, 10.1007/s00376-009-8174-8, 2010a.

Niu, S., Lu, C., Liu, Y., Zhao, L., Lü, J., and Yang, J.: Analysis of the microphysical structure of heavy fog using a droplet spectrometer: A case study, Advances in Atmospheric Sciences, 27, 1259-1275, 10.1007/s00376-010-8192-6, 2010b.

Petters, M. D. and Kreidenweis, S. M.: A single parameter representation of hygroscopic growth and cloud condensation nucleus activity – Part 2: Including solubility, Atmos. Chem. Phys, 2008.

Pilie, R. J., Mack, E. J., Kocmond, W. C., Rogers, C. W. C., and Eadie, W.: The Life Cycle of Valley Fog. Part I: Micrometeorological Characteristics, Journal of Applied Meteorology, 14, 347-363, 1975.

Pilié, R. J., Mack, E. J., Rogers, C. W., Katz, U., and Kocmond, W. C.: The Formation of Marine Fog and the Development of Fog-Stratus Systems along the California Coast, Journal of Applied Meteorology and Climatology, 18, 1275-1286, https://doi.org/10.1175/1520-0450(1979)018<1275:TFOMFA>2.0.CO;2, 1979.

Pruppacher, H. R. and Klett, J. D.: Microstructure of Atmospheric Clouds and Precipitation, in: Microphysics of Clouds and Precipitation, Springer Netherlands, Dordrecht, 10-73, 10.1007/978-0-306-48100-0_2, 2010.

Schwarz, J. P., Gao, R. S., Fahey, D. W., Thomson, D. S., Watts, L. A., Wilson, J. C., Reeves, J. M., Darbeheshti, M., Baumgardner, D. G., Kok, G. L., Chung, S. H., Schulz, M., Hendricks, J., Lauer, A., Kärcher, B., Slowik, J. G., Rosenlof, K. H., Thompson, T. L., Langford, A. O., Loewenstein, M., and Aikin, K. C.: Single-particle measurements

https://doi.org/10.5194/egusphere-2024-2264
Preprint. Discussion started: 16 September 2024

of midlatitude black carbon and light-scattering aerosols from the boundary layer to the lower stratosphere, Journal of Geophysical Research, 111, 10.1029/2006jd007076, 2006.

Shen, C., Zhao, C., Ma, N., Tao, J., Zhao, G., Yu, Y., and Kuang, Y.: Method to Estimate Water Vapor Supersaturation in the Ambient Activation Process Using Aerosol and Droplet Measurement Data, Journal of Geophysical Research: Atmospheres, 123, 10,606-610,619, https://doi.org/10.1029/2018JD028315, 2018.

Shingler, T., Dey, S., Sorooshian, A., Brechtel, F. J., Wang, Z., Metcalf, A., Coggon, M., Mülmenstädt, J., Russell, L. M., Jonsson, H. H., and Seinfeld, J. H.: Characterisation and airborne deployment of a new counterflow virtual impactor inlet, Atmos. Meas. Tech., 5, 1259-1269, 10.5194/amt-5-1259-2012, 2012.

Song, J. I., Yum, S. S., Gultepe, I., Chang, K.-H., and Kim, B.-G.: Development of a new visibility parameterization based on the measurement of fog microphysics at a mountain site in Korea, Atmospheric Research, 229, 115-126, https://doi.org/10.1016/j.atmosres.2019.06.011, 2019.

Spiegel, J. K., Zieger, P., Bukowiecki, N., Hammer, E., Weingartner, E., and Eugster, W.: Evaluating the capabilities and uncertainties of droplet measurements for the fog droplet spectrometer (FM-100), Atmos. Meas. Tech., 5, 2237-2260, 10.5194/amt-5-2237-2012, 2012.

Sun, T., Che, H., Qi, B., Wang, Y., Dong, Y., Xia, X., Wang, H., Gui, K., Zheng, Y., Zhao, H., Ma, Q., Du, R., and Zhang, X.: Aerosol optical characteristics and their vertical distributions under enhanced haze pollution events: effect of the regional transport of different aerosol types over eastern China, Atmos. Chem. Phys., 18, 2949-2971, 10.5194/acp-18-2949-2018, 2018.

Tardif, R. and Rasmussen, R. M.: Event-Based Climatology and Typology of Fog in the New York City Region, Journal of Applied Meteorology and Climatology, 46, 1141-1168, https://doi.org/10.1175/JAM2516.1, 2007.

Tuch, T. M., Haudek, A., Müller, T., Nowak, A., Wex, H., and Wiedensohler, A.: Design and performance of an automatic regenerating adsorption aerosol dryer for continuous operation at monitoring sites, Atmos. Meas. Tech., 2, 417-422, 10.5194/amt-2-417-2009, 2009.

Twomey, S.: The nuclei of natural cloud formation part II: The supersaturation in natural clouds and the variation of cloud droplet concentration, Geofisica pura e applicata, 43, 243-249, 10.1007/BF01993560, 1959.

Twomey, S.: The Influence of Pollution on the Shortwave Albedo of Clouds, Journal of Atmospheric Sciences, 34, 1149-1152, https://doi.org/10.1175/1520-0469(1977)034<1149:TIOPOT>2.0.CO;2, 1977.

van der Velde, I. R., Steeneveld, G. J., Wichers Schreur, B. G. J., and Holtslag, A. A. M.: Modeling and Forecasting the Onset and Duration of Severe Radiation Fog under Frost Conditions, Monthly Weather Review, 138, 4237-4253, https://doi.org/10.1175/2010MWR3427.1, 2010.

Yan, S., Zhu, B., Huang, Y., Zhu, J., Kang, H., Lu, C., and Zhu, T.: To what extents do urbanization and air pollution affect fog?, Atmos. Chem. Phys., 20, 5559-5572, 10.5194/acp-20-5559-2020, 2020.

https://doi.org/10.5194/egusphere-2024-2264
Preprint. Discussion started: 16 September 2024

Zhang, J., Xue, H., Deng, Z., Ma, N., Zhao, C., and Zhang, Q.: A comparison of the parameterization schemes of fog visibility using the in-situ measurements in the North China Plain, Atmospheric Environment, 92, 44-50, https://doi.org/10.1016/j.atmosenv.2014.03.068, 2014.

Zhang, Q., Meng, J., Quan, J., Gao, Y., Zhao, D., Chen, P., and He, H.: Impact of aerosol composition on cloud condensation nuclei activity, Atmos. Chem. Phys., 12, 3783-3790, 10.5194/acp-12-3783-2012, 2012.

Zhao, C. and Garrett, T. J.: Effects of Arctic haze on surface cloud radiative forcing, Geophysical Research Letters, 42, 557-564, https://doi.org/10.1002/2014GL062015, 2015.